

Magnetization dynamics induced by ultrashort terahertz radiation: Toward designing spin-based terahertz sensors


I. Korniienko¹, P. Nieves², O. Chubykalo-Fesenko³ and D. Legut^{1,4,*}

¹*IT4Innovations, VŠB - Technical University of Ostrava, 17. listopadu 2172/15, 708 00 Ostrava-Poruba, Czech Republic*

²*Departamento de Física, Universidad de Oviedo, Calle Leopoldo Calvo Sotelo 18, 33007 Oviedo, Spain*

³*Instituto de Ciencia de Materiales de Madrid, ICMN-CSIC, Campus de Cantoblanco, Calle Sor Juana Inés de la Cruz 3, 28049 Madrid, Spain*

⁴*Department of Condensed Matter Physics, Faculty of Mathematics and Physics, Charles University, Ke Karlovu 3, 121 16 Prague 2, Czech Republic*

 (Received 10 February 2023; revised 25 September 2023; accepted 11 December 2023; published 16 January 2024)

A convenient analytical description of an ultrashort terahertz pulse and an analysis of the influence of this pulse on the Zeeman torque dynamics are extremely important tasks due to the potential applications of terahertz radiation. The theoretical expressions proposed in this paper clarify the physics of magnetic dynamics under the action of the magnetic field of a terahertz pulse and show the role of individual parameters of the material and the pulse field in this process. On the basis of the formulas obtained and the available experimental data for fcc-Co film, we analyze the possibilities of recovering information about the magnetic field of the pulse from the observation of magnetization dynamics, as well as the effect of fluence, Gilbert damping, and magnetic anisotropy on the magnetization dynamics induced by ultrashort terahertz radiation. The theoretical framework presented could potentially be used in the design and optimization of a new generation of terahertz detectors based on the magnetic component of the electromagnetic field.

DOI: [10.1103/PhysRevApplied.21.014025](https://doi.org/10.1103/PhysRevApplied.21.014025)

I. INTRODUCTION

Ultrafast manipulation of magnetic order is of great interest to researchers [1–5] due to the requirement to increase the speed of operation of modern devices and simultaneously reduce their size. Terahertz radiation is expected to play one of the key roles in achieving this goal since the magnetic field in the terahertz range is coupled to the spin degree of freedom by the Zeeman interaction and thus enables a highly efficient torque acting on the magnetic system. In the case of a ferromagnetic layer, the magnetic dynamics induced by a pulse is experimentally studied and shows good agreement with atomistic spin-dynamics simulations based on numerical methods [6] but for further technological applications of the experimental technique a general theoretical description of the time dependence of magnetization under the action of a terahertz pulse is still needed.

Another motivation for developing such a theory is due to the development of terahertz emitters and their improvement [7,8], which results in the possibility of wide practical application of this radiation in various fields [9–11] and

which, on the other hand, gives rise to new, even-more-ambitious, scientific goals. One such goal is to create a platform of room-temperature spin-based terahertz building blocks based on novel magnetism and optics concepts. From this perspective, our theory can potentially be used for terahertz detectors [12] which in all their diversity are currently based on sensitivity to only the electric component of the electromagnetic field. Instead, understanding the magnetization-dynamics physics will provide an opportunity to explore and develop methods for detection of the terahertz-magnetic-field component (for example, on the basis of giant magnetoresistance [13] or magneto-optics [6]). Additionally, it might be practical for interpreting the received signal and separating the useful signal from the noise or even for noise reduction [14].

II. THEORY

A. Governing equation

The ultrafast magnetization dynamics induced by ultrashort laser pulses can be described by the Landau-Lifshitz-Bloch (LLB) equation [15] coupled to the two-temperature model (2TM) [16–18]. The dynamics of the magnetization \mathbf{M} (per unit volume) at high temperature is described by

*dominik.legut@vsb.cz

the classical version of the LLB equation as [15]

$$\frac{d\mathbf{M}}{dt} = -\gamma [\mathbf{M} \times \mathbf{H}_{\text{eff}}] + \frac{\gamma \alpha_{\parallel}}{M^2} (\mathbf{M} \cdot \mathbf{H}_{\text{eff}}) \mathbf{M} - \frac{\gamma \alpha_{\perp}}{M^2} [\mathbf{M} \times [\mathbf{M} \times \mathbf{H}_{\text{eff}}]], \quad (1)$$

where $\gamma = 1.76 \times 10^7 \text{ rad s}^{-1} \text{ Oe}^{-1}$ is the gyromagnetic ratio and \mathbf{H}_{eff} is the effective magnetic field given by

$$\mathbf{H}_{\text{eff}} = \mathbf{H}_{\text{THz}} + \mathbf{H} + \mathbf{H}_D + \mathbf{H}_K + \begin{cases} \frac{1}{\chi_{\parallel}} \left(1 - \frac{M^2}{M_e^2}\right) \mathbf{M}, & T \lesssim T_C, \\ -\frac{1}{\chi_{\parallel}} \left(1 + \frac{3T_C M^2}{5M_0^2 (T - T_C)}\right) \mathbf{M}, & T \gtrsim T_C, \end{cases} \quad (2)$$

where \mathbf{H} is the applied magnetic field, \mathbf{H}_{THz} is the magnetic component of the ultrashort terahertz laser pulse, \mathbf{H}_D is the demagnetizing field, \mathbf{H}_K is the anisotropy field, T_C is the Curie temperature, and $M_0 = \mu_{\text{at}}/v_{\text{at}}$ (where μ_{at} is the atomic moment and v_{at} is the atomic volume) is the saturation magnetization at zero temperature. The equilibrium magnetization at temperature T , $M_e(T)$, is obtained with use of the mean-field approximation (MFA) as the solution of the equation $m_e(T) = L(J_0 m_e/k_B T)$, where $L(x) = \coth(x) - 1/x$ is the Langevin function, $m_e(T) = M_e(T)/M_0$, k_B is the Boltzmann constant, and J_0 is the zero Fourier component (the zeroth moment) of the exchange interaction, which is related to T_C through the MFA as $J_0 = 3k_B T_C$. The longitudinal susceptibility χ_{\parallel} is also calculated through the MFA as

$$\chi_{\parallel} = M_0 \begin{cases} \frac{\mu_{\text{at}} L'}{k_B T - J_0 L'}, & T \lesssim T_C, \\ \frac{\mu_{\text{at}} T_C}{J_0 (T - T_C)}, & T \gtrsim T_C, \end{cases} \quad (3)$$

where $L'(x) = dL/dx$ is the derivative of the Langevin function evaluated at $x = J_0 m_e/k_B T$. For the electron-impurity model in the classical limit $S \rightarrow \infty$, the longitudinal and transverse relaxation parameters read [19,20]

$$\alpha_{\parallel} = \lambda M_0 \frac{2T}{3T_C}, \quad (4)$$

$$\alpha_{\perp} = \lambda M_0 \times \begin{cases} 1 - \frac{2T}{3T_C}, & T \lesssim T_C \\ \frac{T}{3T_C}, & T \gtrsim T_C, \end{cases} \quad (5)$$

where λ is the microscopic relaxation coupling to the bath parameter, which is related to the intrinsic scattering spin-flip probabilities. We assume that the magnetic system is

coupled to the electron bath since the pulse is absorbed by electrons, so the temperature in the LLB equation corresponds to the electron-bath temperature ($T = T_e$), which is obtained from the numerical integration of the 2TM given by

$$\begin{aligned} C_e \frac{dT_e}{dt} &= -g_{e\text{-ph}} (T_e - T_{\text{ph}}) + P_{\text{THz}}(t) + f_{se}(\mathbf{M}), \\ C_{\text{ph}} \frac{dT_{\text{ph}}}{dt} &= g_{e\text{-ph}} (T_e - T_{\text{ph}}), \end{aligned} \quad (6)$$

where T_e is the electron's temperature, T_{ph} is the phonon's temperature, C_e and C_{ph} are the specific heats of the electrons and the lattice, $g_{e\text{-ph}}$ is an electron-phonon coupling constant, which determines the rate of energy exchange between the electrons and the lattice, P_{THz} is the deposited laser energy, and f_{se} describes the effect of spin dynamics on the electron temperature [20]:

$$f_{se}(\mathbf{M}) = \frac{\gamma \alpha_{\parallel} J_0}{\mu_{\text{at}} M_0} \mathbf{M} \cdot \mathbf{H}_{\text{eff}} + \gamma \alpha_{\perp} \frac{(\mathbf{M} \times \mathbf{H}_{\text{eff}})^2}{M^2}. \quad (7)$$

To model the terahertz excitation in the 2TM, we use the same expression as Shalaby *et al.* [6]:

$$P_{\text{THz}}(t) = \frac{AF}{\sqrt{2\pi} \tau_{\text{THz}} d} e^{-\frac{t^2}{2\tau_{\text{THz}}^2}}, \quad (8)$$

where A is the absorption coefficient, F is the incident fluence, d is the film thickness, and τ_{THz} is the temporal width of the pulse.

B. Coherent magnetization dynamics

From the point of view of detecting the magnetic component of the terahertz pulse, as in spin-based terahertz sensors, the coherent magnetization dynamics is more relevant than the incoherent magnetization dynamics because it is correlated to the terahertz magnetic field. The coherent magnetization dynamics is driven by the precessional motion [first term on the right-hand side of Eq. (1)] and transverse relaxation [third term on the right-hand side of Eq. (1)], while the second term on the right-hand side of Eq. (1) describes the change in magnitude of the magnetization vector due to laser heat effects. Analytical solutions for magnetization dynamics can provide a deep theoretical understanding of the dependency of this physical phenomenon on all parameters of the terahertz field and material, contrary to numerical simulations, which give the solution only for a particular set of values of the parameters used in the simulation. Such solutions of this kind could potentially be exploited in the engineering of novel emerging spin-based terahertz technology. In general, deriving an exact solution for Eq. (1) is not easy. Below, we explore possible approximated theoretical expressions for the coherent magnetization dynamics

in the time and frequency domains for the low-fluence and moderate-fluence regimes.

1. Time domain

We start by rewriting Eq. (1) in a form compatible with the Landau-Lifshitz-Gilbert (LLG) equation:

$$\frac{d\mathbf{M}}{dt} = -\frac{\gamma}{1+\alpha^2} [\mathbf{M} \times \mathbf{H}_{\text{eff}}] + \frac{\gamma \tilde{\alpha}_{\parallel} M_{s,300\text{ K}}}{M^2} (\mathbf{M} \cdot \mathbf{H}_{\text{eff}}) \mathbf{M} - \frac{\gamma \alpha M_{s,300\text{ K}}}{M^2(1+\alpha^2)} [\mathbf{M} \times [\mathbf{M} \times \mathbf{H}_{\text{eff}}]], \quad (9)$$

where $\alpha = \alpha_{\perp}/M_{s,300\text{ K}}$, $\tilde{\alpha}_{\parallel} = \alpha_{\parallel}/M_{s,300\text{ K}}$, and $M_{s,300\text{ K}} \equiv M_e(300\text{ K})$ is the saturation magnetization at 300 K. To be consistent with the usual Gilbert-damping term in the LLG equation, we write $1 + \alpha^2$ in the denominator of the precessional and transverse relaxation terms, absent in the original LLB equation, which is obviously irrelevant for $\alpha \ll 1$. We note that the last term of the effective field \mathbf{H}_{eff} in Eq. (2), associated with the internal atomistic exchange interaction, gives a null contribution to the coherent magnetization dynamics.

To find an approximated analytical solution of Eq. (9), some assumptions are required. Firstly, an approximation that greatly simplifies the theoretical analysis of the coherent magnetization dynamics during the application of the laser is the assumption that the magnitude of the magnetic component of the terahertz pulse (\mathbf{H}_{THz}) significantly exceeds the value of the demagnetizing, anisotropy, and external fields:

$$|\mathbf{H}_{\text{THz}}| \gg |\mathbf{H} + \mathbf{H}_D + \mathbf{H}_K|. \quad (10)$$

In this case, the behavior of the magnetization on the ultrashort timescale is approximately like the dynamics of a single-domain isotropic sphere, which can be analytically derived [21,22]. For example, this assumption was satisfied in the work of Shalaby *et al.* [6] for fcc Co ($|\mathbf{H}_{\text{THz}}| \sim 10^5$ Oe and $|\mathbf{H} + \mathbf{H}_D + \mathbf{H}_K| \lesssim 10^3$ Oe). Let us take the direction along the O - z axis as the direction of the terahertz magnetic field ($\mathbf{H}_{\text{THz}} = H_{\text{THz}}\mathbf{e}_z$), as shown in Fig. 1.

It is convenient to express the magnetization vector in spherical coordinates given by angles θ and φ as

$$\mathbf{M} = (M \cos \varphi \sin \theta, M \sin \varphi \sin \theta, M \cos \theta), \quad (11)$$

so that under the above conditions, in terms of spherical coordinates, Eq. (9) reads

$$\frac{\partial \theta}{\sin \theta} = -\partial t \frac{\alpha(t) \gamma H_{\text{THz}}(t) M_{s,300\text{ K}}}{M(t)(1+\alpha(t)^2)}, \quad (12)$$

$$\frac{\partial \varphi}{\partial t} = \frac{\gamma H_{\text{THz}}(t)}{1+\alpha(t)^2}, \quad (13)$$

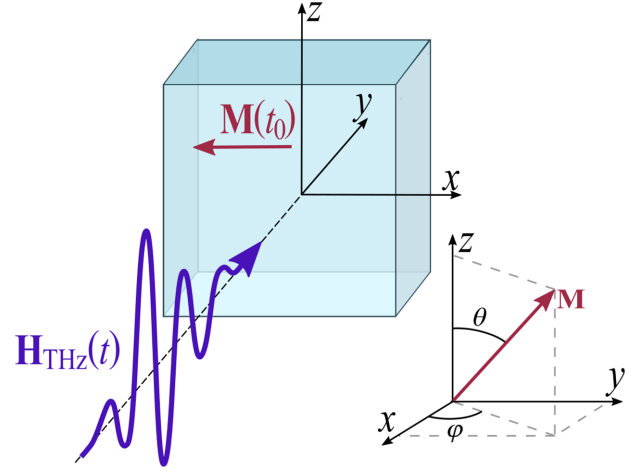


FIG. 1. Schematic diagram of the ferromagnetic thin film sample irradiated by a terahertz magnetic pulse. The sample is magnetized the x - z plane and the initial magnetization $\mathbf{M}(t_0)$ is directed opposite the O - x axis. For better clarity, spherical coordinates θ and φ are shown in the bottom-right corner.

$$\frac{\partial M}{\partial t} = \frac{\gamma \tilde{\alpha}_{\parallel}(t) M_{s,300\text{ K}}}{M(t)} (\mathbf{M}(t) \cdot \mathbf{H}_{\text{eff}}(t)), \quad (14)$$

where Eq. 12 gives the transverse relaxation toward the terahertz magnetic field, Eq. 13 describes the precessional motion around the terahertz magnetic field, and Eq. 14 accounts for the longitudinal relaxation. In general, the time dependence of Gilbert damping $\alpha(t)$ and the magnitude of magnetization $M(t)$ in the transverse relaxation given by Eq. (12) make it difficult to find an analytical solution for coherent dynamics. Hence, we assume temperature-independent Gilbert damping $\alpha(t = t_0)$, which, from the point of view of the LLB framework, is a valid approximation for moderate fluences. Note that such an approximation does not affect significantly the precessional motion in Eq. (13) since typically $\alpha^2(t) \ll 1$. Similarly, in the moderate-fluence regime, the laser-induced demagnetization is low, $M(t)/M_{s,300\text{ K}} \in [0.85, 1]$, see Fig. 2(c), so we set $M(t) \approx M_{s,300\text{ K}}$ in Eq. (12). By these approximations, the LLB equation is reduced to the standard LLG equation, and the differential equations describing coherent dynamics [Eqs. (12) and (13)] take the following approximated forms:

$$\frac{\partial \theta}{\sin \theta} \simeq -\partial t \frac{\alpha \gamma H_{\text{THz}}(t)}{1+\alpha^2}, \quad (15)$$

$$\frac{\partial \varphi}{\partial t} \simeq \frac{\gamma H_{\text{THz}}(t)}{1+\alpha^2}. \quad (16)$$

To model the time dependence of the magnetic field of ultrashort terahertz pulse, we use the following expression:

$$H_{\text{THz}}(t) = H_0 e^{-\beta|t-t_1|} \sin(\omega_0 t + \phi), \quad (17)$$

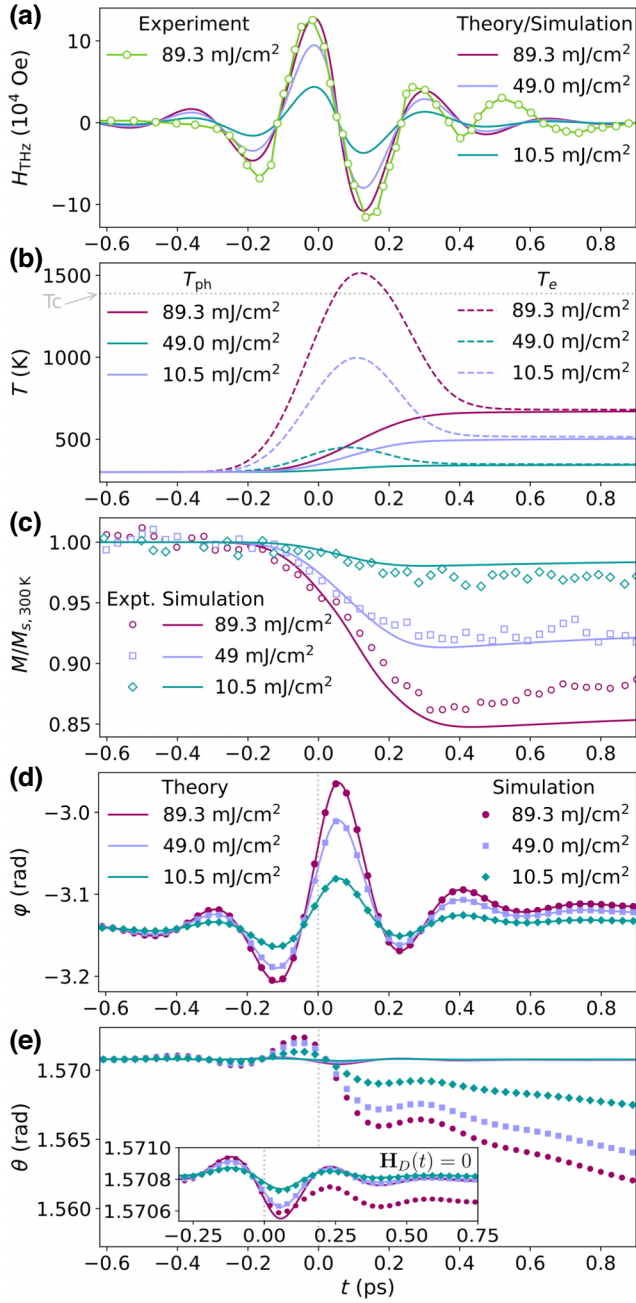


FIG. 2. Time-domain magnetization dynamics driven by ultra-short terahertz pulse for different excitation fluences obtained by simulation (LLB+2TM), theory [Eqs. (18) and (19)], and experiment[6]. (a) Terahertz magnetic pulse inside the Co sample. (b) Time dependence of electronic and phononic temperature bath calculated by the 2TM. (c) Fluence-dependent terahertz-induced demagnetization in Co. (d),(e) Time dependence of polar coordinates under the influence of a magnetic pulse. The inset in (e) shows simulated data for $\theta(t)$ without a demagnetizing field [$\mathbf{H}_D(t) = 0$]. Experimental values for (a),(c) are taken for Co from Ref. [6].

which is simple enough to facilitate the analytical derivation of the coherent magnetization dynamics, and contains all required parameters to adjust the magnetic field shape to

make it as close as possible to the experimental one. Here, w_0 is the angular frequency, H_0 is the parameter responsible for the magnitude of the amplitude and that depends on the laser fluence, β is responsible for the decay of the wave in the pulse, and the parameters t_1 and ϕ give the time shifts. Insertion of Eq. (17) into Eqs. (15) and (16) and our solving these differential equations leads to

$$\theta(t) = 2 \arctan \left(\exp \left(C_\theta - \frac{\alpha\gamma}{1 + \alpha^2} \frac{H_0}{w_0^2 + \beta^2} \left(-e^{-\beta|t-t_1|} (w_0 \cos(w_0 t + \phi)) + \frac{|t-t_1|}{t-t_1} \beta \sin(w_0 t + \phi) \right) + \frac{|t-t_1|}{t-t_1} \beta \sin(w_0 t_1 + \phi) \right) \right) \quad (18)$$

and

$$\varphi(t) = C_\varphi + \frac{\gamma}{1 + \alpha^2} \frac{H_0}{w_0^2 + \beta^2} \left(-e^{-\beta|t-t_1|} (w_0 \cos(w_0 t + \phi)) + \frac{|t-t_1|}{t-t_1} \beta \sin(w_0 t + \phi) + \frac{|t-t_1|}{t-t_1} \beta \sin(w_0 t_1 + \phi) \right). \quad (19)$$

The constants of integration can be found from the initial conditions and pulse parameters:

$$C_\theta = \ln \left| \tan \left(\frac{\theta(t_0)}{2} \right) \right| + \frac{\alpha\gamma}{1 + \alpha^2} \frac{H_0}{w_0^2 + \beta^2} \left(e^{\beta(t_0-t_1)} (-w_0 \cos(w_0 t_0 + \phi)) + \beta \sin(w_0 t_0 + \phi) - \beta \sin(w_0 t_1 + \phi) \right) \quad (20)$$

and

$$C_\varphi = \varphi(t_0) + \frac{\gamma}{1 + \alpha^2} \frac{H_0}{w_0^2 + \beta^2} \left(\beta \sin(w_0 t_1 + \phi) + e^{\beta(t_0-t_1)} (w_0 \cos(w_0 t_0 + \phi) - \beta \sin(w_0 t_0 + \phi)) \right). \quad (21)$$

The angles $\theta(t_0)$ and $\varphi(t_0)$ determine the equilibrium position of the magnetization vector before the beginning of the influence of the terahertz field (at initial time t_0) and thus are known. For example, in Fig. 1 they are $\theta(t_0) = \pi/2$ and $\varphi(t_0) = -\pi$. In Sec. IV, we carefully study the validity and limitation of all approximations used to derive the analytical solution for $\theta(t)$ and $\varphi(t)$ [Eqs. (18) and (19)] by comparing it with the numerical simulation by the full macrospin LLB+2TM approach described in Sec. II A, which does not contain any approximation and is valid for all fluence regimes.

2. Frequency domain

Inspecting measured data in the frequency domain is an important part of analyzing and monitoring signals. In contrast to the time domain, where the wave is described by the sum of its characteristics, in the frequency domain the characteristics of the signal are described by separate frequencies and thus open up potential opportunities to remove noise, improve signal clarity, and improve data analysis [23].

The Fourier transform of the terahertz-magnetic-pulse equation (17) is given by

$$\begin{aligned}\tilde{H}_{\text{THz}}(\omega) &= \frac{1}{2\pi} \int_{-\infty}^{\infty} H_{\text{THz}}(t) e^{-i\omega t} dt = \\ &= \frac{H_0 \beta}{2\pi i} \left(\frac{e^{-i(\omega - \omega_0)t_1 + i\phi}}{\beta^2 + (\omega - \omega_0)^2} - \frac{e^{-i(\omega + \omega_0)t_1 - i\phi}}{\beta^2 + (\omega + \omega_0)^2} \right).\end{aligned}\quad (22)$$

Similarly, an expression for the Fourier transform of the angle φ in Eq. (19) can be obtained:

$$\begin{aligned}\tilde{\varphi}(\omega) &= \frac{\gamma H_0 \beta}{(1 + \alpha^2)(\omega_0^2 + \beta^2)} \left(\frac{(\omega - 2\omega_0)e^{-i(\omega - \omega_0)t_1 + i\phi}}{\beta^2 + (\omega - \omega_0)^2} - \right. \\ &\quad \left. - \frac{(\omega + 2\omega_0)e^{-i(\omega + \omega_0)t_1 - i\phi}}{\beta^2 + (\omega + \omega_0)^2} \right).\end{aligned}\quad (23)$$

To obtain Eq. (23), we left in the expression for $\varphi(t)$ [Eq. (19)] only time-dependent terms because the constants lead only to the appearance of the δ function and do not provide new information. Unfortunately, the complexity of Eq. (18) does not allow us to obtain a similar expression for $\theta(\omega)$.

III. MODEL PARAMETERS

To apply the theoretical framework described in Sec. II, we consider the experimental and modeling results reported by Shalaby *et al.* [6] for fcc-Co thin film. Namely, we set the following values for the material parameters: $T_C = 1388$ K, $\mu_{\text{at}} = 1.72\mu_B$, $M_{s,0\text{ K}} = M_0 = 1446$ emu/cm³, $M_{s,300\text{ K}} = m_e(T = 300\text{ K})M_0$, $d = 15$ nm, $C_{\text{ph}} = 3.8 \times 10^6$ J/m³ K, $C_e(T_e) = \gamma_e T_e$, $\gamma_e = 400$ J/m³ K², and $g_{ep} = 4 \times 10^{18}$ W/m³ K. The system is at room temperature before the laser is applied: $T_e(t_0) = T_{\text{ph}}(t_0) = 300$ K. The atomistic coupling parameter λ is set to 0.00216 so that the Gilbert damping is given by $\alpha = \alpha_{\perp}/M_{s,300\text{ K}}(t = t_0, T = 300\text{ K}) = 0.002$ as in the work of Shalaby *et al.* [6] and works [24,25]. A case with larger Gilbert damping is considered in Sec. IV C. The magnetic anisotropy is assumed to be uniaxial with easy axis perpendicular to the thin film (easy axis parallel to the y axis

[26]:

$$\mathbf{H}_K = \frac{2K_u}{M^2} (\mathbf{M} \cdot \mathbf{e}_K) \mathbf{e}_K, \quad (24)$$

where we used the temperature-dependent anisotropy scaled as $K_u = K_{u,0}m(T)^3$, where $m = M/M_0$ is the reduced magnetization, $K_{u,0} = 2.2 \times 10^5$ erg/cm³, and $\mathbf{e}_K = (0, 1, 0)$. A constant external magnetic field $\mathbf{H} = (-200, 0, 0)$ Oe is applied to set the equilibrium magnetization at initial time t_0 along the direction $(-1, 0, 0)$; see Fig. 1. A case with larger magnetic anisotropy and external magnetic field is discussed in Sec. IV C. For the demagnetizing field, we use the shape factor of a uniformly magnetized thin film [27]:

$$\mathbf{H}_D = -4\pi (\mathbf{M} \cdot \mathbf{e}_K) \mathbf{e}_K. \quad (25)$$

Regarding the terahertz pulse, we study three fluence cases, $F = 10.5, 49, \text{ and } 89.3$ mJ/cm², which correspond to the lowest, intermediate, and highest values used in Ref. [6], respectively. The temporal width of the pulse τ_{THz} is 110 fs, while the absorption coefficient A was decreased to 0.035 with respect to Ref. [6] ($A = 0.11$) so as to obtain similar laser-induced demagnetization curves as in the experiment for all fluences; see Fig. 2(c). The parameters of the terahertz magnetic field for fluence $F = 89.3$ mJ/cm² are obtained by our fitting Eq. (17) to the experimental data in Ref. [6] for the same fluence, as shown in Fig. 2(a). This procedure gives $H_0 = 185441$ Oe, $\beta = 5.822 \times 10^{12}$ s⁻¹, $t_1 = 0.042 \times 10^{-12}$ s, $\omega_0 = 18.039 \times 10^{12}$ rad/s (or $f_0 = \omega_0/2\pi = 2.871$ THz), and $\phi = -4.173$ rad. For the other-two fluence cases, we rescaled H_0 according to $H_0^2(F')/F' = H_0^2(F)/F$, which approximately follows from [6] $P_{\text{THz}}(t) \sim E_{\text{THz}}(t)^2 \propto H_{\text{THz}}(t)^2$.

The simulations correspond to the numerical integration of the LLB equation [Eq. (1)] with one macrospin coupled to the 2TM [Eq. (6)] using Heun's method with time step $dt = 0.1$ fs, while the initial time is $t_0 = -1$ ps. Variable time and temperature relaxation parameters are included in the simulation via Eqs. (4) and (5), but not in the theoretical equations (18) and (19), where α is assumed to be constant: $\alpha(t) = \alpha(t_0)$.

IV. RESULTS

The presented theoretical framework may be applied in different ways depending on the known data. Here, we analyze two possible situations where this theory could be helpful: (i) we know everything about the terahertz magnetic pulse and want to know what magnetization dynamics it will cause (Sec. IV A) or (ii) we know the dynamics of magnetization and want to know everything about the terahertz magnetic pulse that caused it (Sec. IV B). We also

study the cases with large time-dependent Gilbert damping and high magnetic anisotropy (Sec. IV C) to verify the range of applicability of the approximations used in the derivation of the analytical formulas for the coherent dynamics [Eqs. (18) and (19)].

A. Magnetization dynamics driven by an ultrashort terahertz pulse

A comparison between the theoretical expression for coherent dynamics [Eqs. (18) and (19)], simulation by the LLB+2TM approach (Sec. II A), and experiment (Ref. [6]) is shown in Figs. 2 and 3. We observe that the theoretical precessional motion $\varphi(t)$ described by Eq. (19) is in very good agreement with the simulated data, see Fig. 2(d), validating the approximations used in Sec. II B 1. In Fig. 2(e) we see that the theoretical transverse relaxation toward the terahertz magnetic field $\theta(t)$ described by Eq. (18) cannot reproduce the data simulated with the LLB+2TM approach. This deviation on $\theta(t)$ is related mainly to the demagnetizing field \mathbf{H}_D , which does not influence $\varphi(t)$ on the pulse-duration timescale. To see this, we plot the simulated data for $\theta(t)$ without the demagnetizing field ($\mathbf{H}_D(t) = 0$) in the inset in Fig. 2(e), finding much-better agreement between theory and simulation. In this case, deviation between theory and simulation is observed only in the highest-fluence case, $F = 89.3 \text{ mJ/cm}^2$, due to the time dependence of the Gilbert damping $\alpha(t)$, which is not included in the derivation of Eq. (18). Unfortunately, the lack of experimental data for $\theta(t)$ does not allow us to conclude if this model provides a realistic description of the transverse relaxation under these conditions. The small observed change in $\theta(t)$ on an ultrashort timescale is associated with the low Gilbert damping of this material, $\alpha \sim 0.002$. We verified that the anisotropy and external

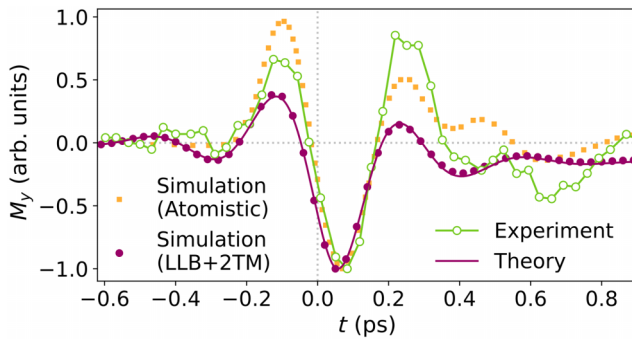


FIG. 3. Theoretical magnetization time dependence [Eqs. (11), (18), (19)] compared with calculated results from simulations and with experimental results for fluence $F = 89.3 \text{ mJ/cm}^2$. The data are normalized with respect to the maximum value of M_y . Experimental data and atomistic simulation data are taken from Ref. [6].

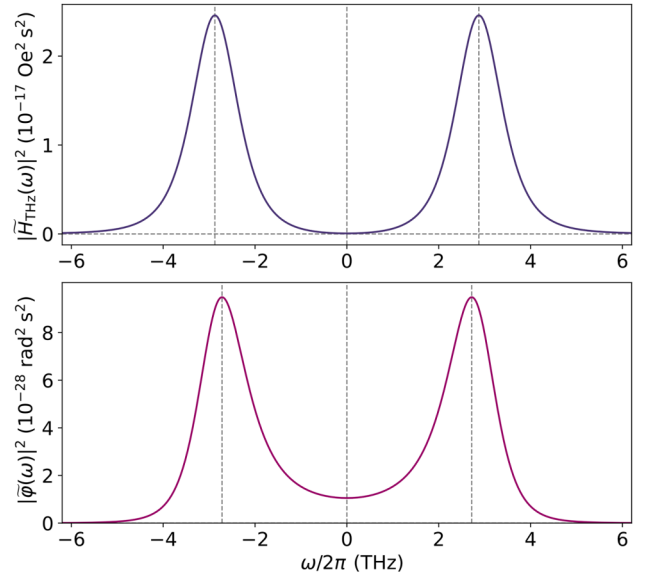


FIG. 4. Frequency-domain terahertz magnetic field and spherical-coordinate φ spectrum for the case with fluence $F = 89.3 \text{ mJ/cm}^2$. Frequencies at which maxima are observed are marked by dashed lines. For the upper graph these frequencies are 2.874 and -2.874 THz and for the lower graph they are 2.718 and -2.718 THz .

magnetic fields do not significantly influence the dynamics during the application of the ultrashort terahertz pulse ($t \lesssim 1 \text{ ps}$), but can do it at longer timescales during the recovery of magnetization to the initial equilibrium state. The effects of larger Gilbert damping and magnetic anisotropy are discussed in Sec. IV C. The theoretical magnetization component M_y and the simulated magnetization component M_y follow the same pattern as in the experiment and atomistic spin-dynamics simulations given in Ref. [6] for the case with fluence $F = 89.3 \text{ mJ/cm}^2$; see Fig. 3.

The frequency-domain analysis of the terahertz magnetic pulse H_{THz} and for the spherical coordinate of magnetization φ for the case with fluence $F = 89.3 \text{ mJ/cm}^2$ is shown in Fig. 4. It should be noted that the maximum in the spectrum of the field H_{THz} is observed not strictly at frequency ω_0 ; this is related to the shape of the magnetic pulse. For example, in Fig. 4, maxima for $|\tilde{H}_{\text{THz}}(\omega)|^2$ are observed at frequencies of 2.874 and -2.874 THz , while the frequency for the given pulse from Eq. (17) is, as mentioned above, 2.871 THz. An even-greater difference from this frequency is observed for maxima in the spectrum of φ . These maxima corresponds to frequencies of 2.718 and -2.718 THz and are thus closer to the value of $\sqrt{(\omega_0^2 - \beta^2)}/2\pi = 2.717 \text{ THz}$. The widths of the peaks are related to the decay parameter β , and for $\beta \rightarrow 0$ we get Dirac δ functions of ω_0 in both spectra.

B. Recovery of the terahertz-pulse field through the analysis of magnetization dynamics

Another interesting question is the possibility of recovering all the information about the magnetic pulse from the observed magnetization dynamics. For this purpose, the mathematically simplest solution is to use Eq. (15) or Eq. (16) directly. Thus, for example, for a given experimental set of points $\theta(t_i)$ or $\varphi(t_i)$ at time t_i , it is easy to obtain from Eq. (15) or Eq. (16) a set of terahertz-magnetic-field values at these times as

$$H_{\text{THz}}(t_i) = -\frac{(1 + \alpha^2)(\theta(t_i) - \theta(t_{i-1}))}{\alpha\gamma(t_i - t_{i-1}) \sin(\theta(t_i))} \quad (26)$$

or

$$H_{\text{THz}}(t_i) = \frac{(1 + \alpha^2)(\varphi(t_i) - \varphi(t_{i-1}))}{\gamma(t_i - t_{i-1})}. \quad (27)$$

Comparison of the points obtained with Eq. (17) can give us more-comprehensive information about the initial terahertz magnetic pulse.

However, as can be seen from Fig. 2(e), the changes in the angle θ can be so small that it can become problematic to measure them experimentally. Thus, it is practical to recover the shape of the terahertz magnetic field of the pulse from the precessional motion (angle φ). For this purpose, it is necessary to use the analytical expression for

$\varphi(t)$ given by Eq. (19), which contains a set of unknown parameters that can be obtained by fitting it to the experimental data. Experimental data given in arbitrary units (see Fig. 3) do not allow us to determine the value of $\varphi(t)$, so we used a more-general and more-complex approach with Eqs. (11), (18), and (19) and the program GNUPLOT [28] for this task and obtained the following values of the unknown parameters: $H_0 = 919108$ Oe, $\beta = 2.92 \times 10^{12} \text{ s}^{-1}$, $t_1 = 1.88 \times 10^{-16} \text{ s}$, $w_0 = 18.62 \times 10^{12} \text{ rad/s}$, and $\phi = -4.467$ rad. It should be noted that in the case of use of arbitrary units for magnetization components, the amplitude parameter H_0 is used as a fitting parameter and does not provide any information about the true value of the amplitude of the pulse field. With the parameters obtained, using Eq. (17), one can restore the magnetic pulse field [solid blue line in Fig. 5(a)].

C. Influence of Gilbert damping and magnetic anisotropy

In our derivation of the theoretical expressions for the coherent dynamics [Eqs. (18) and (19)] we used two approximations associated with (i) Gilbert damping by ignoring its time (temperature) dependence $\alpha = \alpha_{\perp}/M_{s,300 \text{ K}}(t_0)$ and (ii) magnetic anisotropy [Eq. (24)]. Hence, it is worth investigating the effect of these parameters on the coherent dynamics systematically. In Sec. IV A, we studied the case with low Gilbert damping ($\alpha = 0.002$)

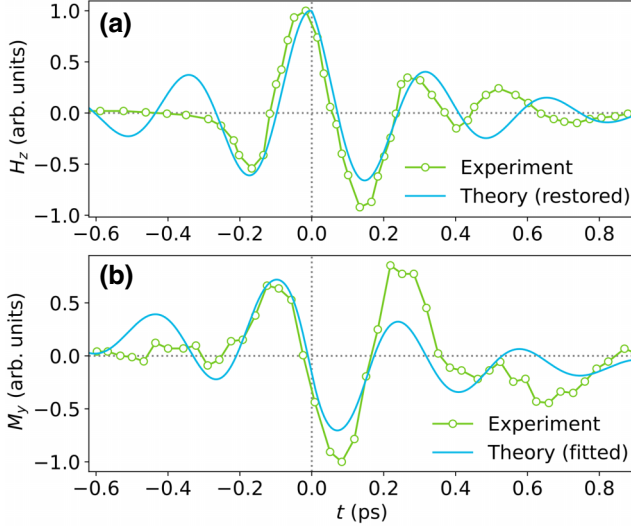


FIG. 5. Recovery of the magnetic field of the terahertz pulse based on experimental measurements of the magnetization precessional motion for fcc Co. The theoretical dependence (solid blue line) is obtained by our fitting the experimental data [6] for the time dependence of the magnetization component M_y in (b) (green circles) to Eq. (11), taking into account Eqs. (18)–(20), and finding the field parameters H_0 , w_0 , β , t_1 , and ϕ for recovery by Eq. (17), which are then used in (a). For the calculations, we consider α to be 0.002.

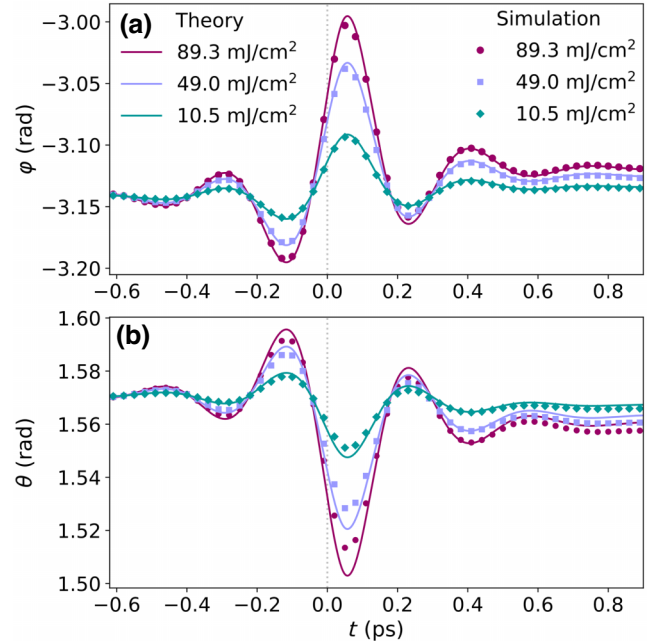


FIG. 6. Terahertz-pulse-induced magnetization dynamics for different excitation fluences in the case of large Gilbert damping [$\alpha(t_0) = 0.464$] and low anisotropy ($K_{u,0} = 2.2 \times 10^5 \text{ erg/cm}^3$). The time dependences of polar coordinates φ and θ are shown in (a),(b), respectively.

and low magnetic anisotropy ($K_{u,0} = 2.2 \times 10^5$ erg/cm³). In this section, we use the same model parameters described in Sec. III, and we only increase Gilbert damping or/and magnetic anisotropy (jointly with the constant external magnetic field to stabilize initial magnetization).

1. Large Gilbert damping and low magnetic anisotropy

We first study the case of large Gilbert damping and low magnetic anisotropy. To this end, we increase the atomistic coupling parameter λ up to 0.5 so that Gilbert damping at the initial time is given by $\alpha = \alpha_{\perp}/M_{s,300\text{K}}(t_0) = 0.464$. Such a large value can be found in multilayer systems such as Pt/Co/Pt [25,29]. Note that the LLB equation (and in principle the LLG equation) can be derived only for weak spin coupling to the bath [15].

We keep the same low anisotropy $K_{u,0} = 2.2 \times 10^5$ erg/cm³ as in fcc Co, and low external magnetic

field $\mathbf{H} = (-200, 0, 0)$ Oe. The results for this case are presented in Fig. 6. We observe that the theoretical expressions for the coherent dynamics [Eqs. (18) and (19)] are in quite good agreement with the simulations for the fluence cases considered. Interestingly, now the maximum change in $\theta(t)$ is significantly larger ($\Delta\theta \sim 0.1$ rad) and is of the same order of magnitude as the maximum change in $\varphi(t)$. Hence, this suggests that it might be possible to experimentally measure the field of ultrashort terahertz pulse through the transverse relaxation $\theta(t)$ in materials with large Gilbert damping, opening new ways to detect the terahertz pulse signals beyond the precessional motion $\varphi(t)$.

2. Low Gilbert damping and large magnetic anisotropy

We now study the case of low Gilbert damping $\alpha = 0.002$ and large uniaxial magnetic anisotropy $K_{u,0} = 2.2 \times 10^7$ erg/cm³ under a large external field

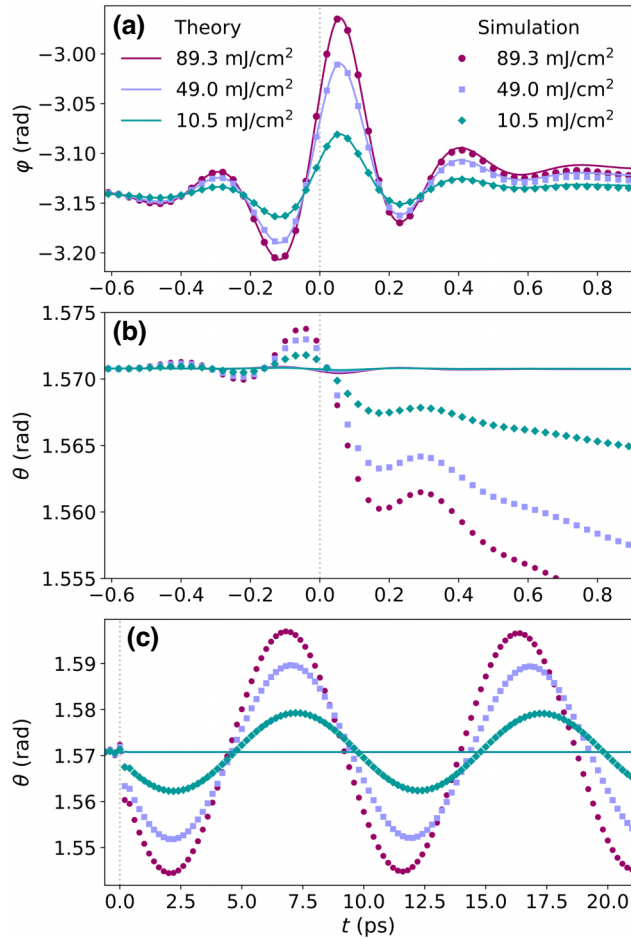


FIG. 7. Terahertz-pulse-induced magnetization dynamics for different excitation fluences in the case of low Gilbert damping ($\alpha = 0.002$) and large anisotropy ($K_{u,0} = 2.2 \times 10^7$ erg/cm³). (a),(b) Time dependence of the polar coordinates φ and θ under the influence of the terahertz pulse. (c) Transverse relaxation $\theta(t)$ on a long timescale.

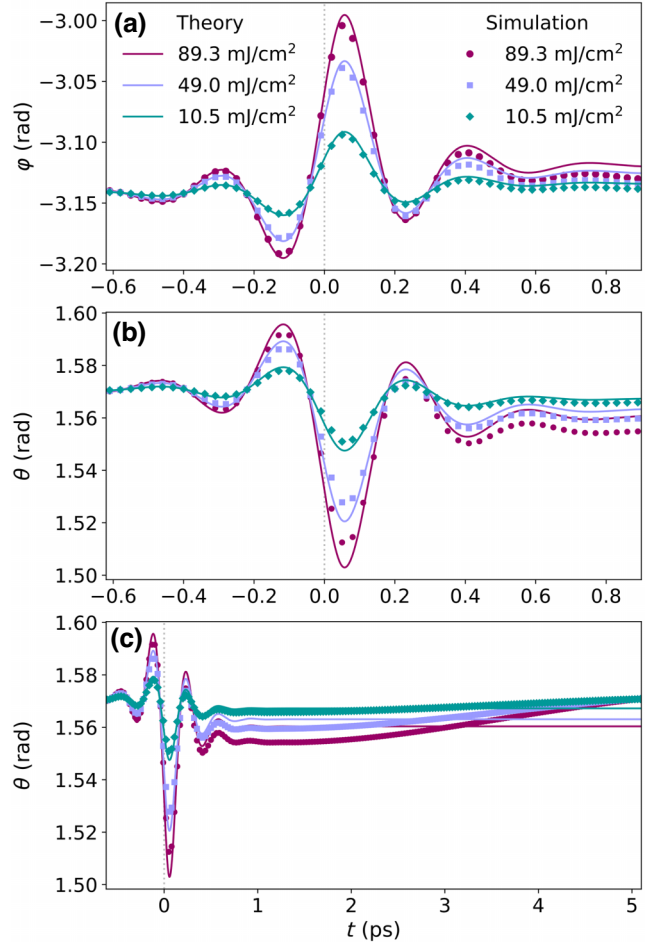


FIG. 8. Terahertz-pulse-induced magnetization dynamics for different excitation fluences in the case of large Gilbert damping ($\alpha = 0.464$) and large anisotropy ($K_{u,0} = 2.2 \times 10^7$ erg/cm³). (a) Precessional motion $\varphi(t)$ and (b) transverse relaxation $\theta(t)$ under the influence of an ultrashort terahertz pulse. (c) $\theta(t)$ on a long timescale.

$H = (-40\,000, 0, 0)$ Oe to stabilize the initial magnetization along the direction $(-1, 0, 0)$; see Fig. 1. A comparison between theory [Eqs. (18) and (19)] and simulation is shown in Fig. 7. Here, we see good agreement only for the precessional motion $\varphi(t)$ but not for the transverse relaxation $\theta(t)$. The dynamics on a long timescale ($t > 1$ ps) is driven by the external, demagnetizing, and anisotropy fields, and exhibits an oscillating behavior that decays slowly with time due to low Gilbert damping until the initial equilibrium magnetic direction is recovered. Such dynamics is described by the simulation but not by the theoretical formulas for the coherent dynamics [Eqs.(18) and (19)] since these fields were not included [Eq. (10)].

3. Large Gilbert damping and large magnetic anisotropy

Lastly, we study the case of large Gilbert damping $\alpha(t = t_0) = 0.464$ and large uniaxial magnetic anisotropy $K_{u,0} = 2.2 \times 10^7$ erg/cm³ under a large external field $H = (-40\,000, 0, 0)$ Oe to stabilize the initial magnetization along the direction $(-1, 0, 0)$. For example, such a combination of large values can be found in L1₀ Fe-Pt films [30,31]. In Fig. 8, we present the theoretical results [Eqs. (18) and (19)] jointly with the simulated data for this case. We observe consistent results between the two approaches for both the precessional dynamics and the transverse dynamics. On a longer timescale ($t > 1$ ps), $\theta(t)$ does not exhibit significant oscillating behavior, since it decays much faster with time due to its large Gilbert damping.

V. DISCUSSION AND CONCLUSION

Analysis of the results obtained shows good agreement with simulation based on numerical methods and good agreement of magnetization behavior with experimental data, but with a some mismatches in the magnitude of the field-induced magnetization deviations. However, phenomena that we ignored (error bars in the experimental data, boundary conditions that can have a significant effect in the case of thin films, the spatial dependence of the magnetic field inside the sample, etc.) can also be responsible for contributing to this deviation. Additionally, we cannot exclude the possible existence of additional spin-orbit torques, induced by absorption of the terahertz electromagnetic field [32,33]. Thus, questions about taking into account all these effects lead to new tasks for further research.

In the issue of pulse-information recovery by observation of magnetization, as can be seen from Fig. 6, for a material with a large Gilbert-damping parameter α (approximately 10^{-1}), the changes in the magnitude of the angle θ can be quite large (of the same order of magnitude as the changes in φ), and thus, for these materials, it is possible to restore the shape of the magnetic field both from magnetization precessional motion and from transverse relaxation. In other words, in this case it might be

possible to detect terahertz radiation from the magnetization component parallel to the terahertz field \mathbf{H}_{THz} , opening new ways to detect the terahertz pulse signals beyond the precessional motion $\varphi(t)$, while for materials with small α (approximately 10^{-3}), field detection is possible only from the precessional motion since the change in θ is too small.

In summary, we have presented a general theoretical model for the magnetization dynamics induced by ultrashort terahertz radiation that agrees with simulation based on the numerical method. We have analyzed the influence of the magnitudes of the terahertz-pulse fluence, magnetic anisotropy, and Gilbert damping on it. We have obtained the frequency spectrum of the radiation for a terahertz magnetic pulse, and have analyzed the possibility of recovering all the information about the magnetic field of the terahertz pulse based on the known time dependence of the magnetization component (or components).

The analysis of the effects of Gilbert damping and magnetic anisotropy on the coherent dynamics reveals a rich variety of different magnetic responses to ultrashort terahertz radiation on transverse relaxation θ , while the precessional motion φ is not significantly affected by these parameters. However, they could play an important role in terahertz detection through transverse relaxation, so our results constitute a step forward in designing novel spin-based terahertz sensors.

ACKNOWLEDGMENTS

This work was supported by e-INFRA CZ (ID:90254) and QM4St project No. CZ.02.01.01/00/22_008/0004572 of the Ministry of Education, Youth and Sports of the Czech Republic and by Project No. 22-35410K and No. 23-04746S of the Czech Science Foundation. This work has received funding from the European Union's Horizon 2020 research and innovation program under Grant Agreement No. 863155. P.N. acknowledges support from Grant No. MU-23-BG22/00168 funded by the Ministry of Universities of Spain. We thank A.L. Chekhov, T. Kampfrath and U. Nowak for fruitful discussions.

-
- [1] A. Kirilyuk, A. V. Kimel, and T. Rasing, Ultrafast optical manipulation of magnetic order, *Rev. Mod. Phys.* **82**, 2731 (2010).
 - [2] K. Olejník, T. Seifert, Z. Kašpar, V. Novák, P. Wadley, R. P. Campion, M. Baumgartner, P. Gambardella, P. Němec, J. Wunderlich, J. Sinova, P. Kužel, M. Müller, T. Kampfrath, and T. Jungwirth, Terahertz electrical writing speed in an antiferromagnetic memory, *Sci. Adv.* **4**, eaar3566 (2018).
 - [3] U. Ritzmann, P. Baláž, P. Maldonado, K. Carva, and P. M. Oppeneer, High-frequency magnon excitation due to femtosecond spin-transfer torques, *Phys. Rev. B* **101**, 174427 (2020).

- [4] X. Liu, E. Jal, R. Delaunay, R. Jarrier, G. S. Chiuzbaian, G. Malinowski, T. Golz, E. Zapolnova, R. Pan, N. Stojanovic, J. Lüning, and B. Vodungbo, Investigating coherent magnetization control with ultrashort THz pulses, *Appl. Sci.* **12**, 1323 (2022).
- [5] T. Chirac, J.-Y. Chauleau, P. Thibaudeau, O. Gomonay, and M. Viret, Ultrafast antiferromagnetic switching in NiO induced by spin transfer torques, *Phys. Rev. B* **102**, 134415 (2020).
- [6] M. Shalaby, A. Donges, K. Carva, R. Allenspach, P. M. Oppeneer, U. Nowak, and C. P. Hauri, Coherent and incoherent ultrafast magnetization dynamics in 3d ferromagnets driven by extreme terahertz fields, *Phys. Rev. B* **98**, 014405 (2018).
- [7] T. Seifert, *et al.*, Efficient metallic spintronic emitters of ultrabroadband terahertz radiation, *Nat. Photonics* **10**, 483 (2016).
- [8] J. Hawecker, E. Rongione, A. Markou, S. Krishnia, F. Godel, S. Collin, R. Lebrun, J. Tignon, J. Mangeney, T. Boulier, J.-M. George, C. Felser, H. Jaffrès, and S. Dhillon, Spintronic THz emitters based on transition metals and semi-metals/Pt multilayers, *Appl. Phys. Lett.* **120**, 122406 (2022).
- [9] S. S. Dhillon, *et al.*, The 2017 terahertz science and technology roadmap, *J. Phys. D: Appl. Phys.* **50**, 043001 (2017).
- [10] X. Lu, S. Venkatesh, and H. Saeidi, A review on applications of integrated terahertz systems, *China Commun.* **18**, 175 (2021).
- [11] A. Y. Pawar, D. D. Sonawane, K. B. Erande, and D. V. Derle, Terahertz technology and its applications, *Drug Invent. Today* **5**, 157 (2013).
- [12] R. A. Lewis, A review of terahertz detectors, *J. Phys. D: Appl. Phys.* **52**, 433001 (2019).
- [13] P. P. Freitas, R. Ferreira, and S. Cardoso, Spintronic sensors, *Proc. IEEE* **104**, 1894 (2016).
- [14] M. Jotta Garcia, J. Moulin, S. Wittrock, S. Tsunegi, K. Yakushiji, A. Fukushima, H. Kubota, S. Yuasa, U. Ebels, M. Pannetier-Lecoecur, C. Fermon, R. Lebrun, P. Bortolotti, A. Solognac, and V. Cros, Spin-torque dynamics for noise reduction in vortex-based sensors, *Appl. Phys. Lett.* **118**, 122401 (2021).
- [15] D. A. Garanin, Fokker-Planck and Landau-Lifshitz-Bloch equations for classical ferromagnets, *Phys. Rev. B* **55**, 3050 (1997).
- [16] U. Atxitia, O. Chubykalo-Fesenko, J. Walowski, A. Mann, and M. Münzenberg, Evidence for thermal mechanisms in laser-induced femtosecond spin dynamics, *Phys. Rev. B* **81**, 174401 (2010).
- [17] U. Atxitia, D. Hinzke, and U. Nowak, Fundamentals and applications of the Landau-Lifshitz-Bloch equation, *J. Phys. D: Appl. Phys.* **50**, 033003 (2016).
- [18] J. Mendil, P. Nieves, O. Chubykalo-Fesenko, J. Walowski, T. Santos, S. Pisana, and M. Münzenberg, Resolving the role of femtosecond heated electrons in ultrafast spin dynamics, *Sci. Rep.* **4**, 3980 (2014).
- [19] P. Nieves, D. Serantes, U. Atxitia, and O. Chubykalo-Fesenko, Quantum Landau-Lifshitz-Bloch equation and its comparison with the classical case, *Phys. Rev. B* **90**, 104428 (2014).
- [20] P. Nieves, D. Serantes, and O. Chubykalo-Fesenko, Self-consistent description of spin-phonon dynamics in ferromagnets, *Phys. Rev. B* **94**, 014409 (2016).
- [21] J. D. Hannay, Ph.D. thesis, University of Wales, 2001.
- [22] R. F. L. Evans, W. J. Fan, P. Churemart, T. A. Ostler, M. O. A. Ellis, and R. W. Chantrell, Atomistic spin model simulations of magnetic nanomaterials, *J. Phys. Condens. Matter* **26**, 103202 (2014).
- [23] A. A. Chauvet, in *Fourier Transforms*, edited by G. S. Nikoli and D. Z. Markovi-Nikoli (IntechOpen, Rijeka, 2019), Chap. chapter 6..
- [24] L. van Bockstal and F. Herlach, Ferromagnetic relaxation in 3d metals at far infrared frequencies in high magnetic fields, *J. Phys. Condens. Matter* **2**, 7187 (1990).
- [25] E. Barati, M. Cinal, D. M. Edwards, and A. Umerski, Gilbert damping in magnetic layered systems, *Phys. Rev. B* **90**, 014420 (2014).
- [26] J. Goddard and J. G. Wright, Magnetic anisotropy in electrodeposited single crystal films of cobalt, *Br. J. Appl. Phys.* **16**, 1251 (1965).
- [27] J. M. D. Coey, *Magnetism and Magnetic Materials* (Cambridge University Press, New York, 2010).
- [28] T. Williams and C. Kelley, many others, Gnuplot 5.4: An interactive plotting program, <http://gnuplot.sourceforge.net/> (2022).
- [29] S. Mizukami, E. P. Sajitha, D. Watanabe, F. Wu, T. Miyazaki, H. Naganuma, M. Oogane, and Y. Ando, Gilbert damping in perpendicularly magnetized Pt/Co/Pt films investigated by all-optical pump-probe technique, *Appl. Phys. Lett.* **96**, 152502 (2010).
- [30] X. Ma, L. Ma, P. He, H. B. Zhao, S. M. Zhou, and G. Lüpke, Role of antisite disorder on intrinsic Gilbert damping in Γ_1 FePt films, *Phys. Rev. B* **91**, 014438 (2015).
- [31] K.-D. Lee, H.-S. Song, J.-W. Kim, H. S. Ko, J.-W. Sohn, B.-G. Park, and S.-C. Shin, Gilbert damping and critical real-space trajectory of Γ_1 -ordered FePt films investigated by magnetic-field-induction and all-optical methods, *Appl. Phys. Express* **7**, 113004 (2014).
- [32] F. Freimuth, S. Blügel, and Y. Mokrousov, Laser-induced torques in metallic ferromagnets, *Phys. Rev. B* **94**, 144432 (2016).
- [33] F. Freimuth, S. Blügel, and Y. Mokrousov, Laser-induced torques in metallic antiferromagnets, *Phys. Rev. B* **103**, 174429 (2021).